



HAL
open science

Numerical modeling of the impact of leakage under divertor baffle in WEST

Hao Yang, Guido Ciruolo, Hugo Bufferand, Jérôme Bucalossi, Nicolas Fedorczak, Patrick Tamain, G. Falchetto, Nicolas Rivals, J.P. Gunn, Yannick Marandet, et al.

► **To cite this version:**

Hao Yang, Guido Ciruolo, Hugo Bufferand, Jérôme Bucalossi, Nicolas Fedorczak, et al.. Numerical modeling of the impact of leakage under divertor baffle in WEST. PSI 25 - 25th International Conference on Plasma Surface Interaction in Controlled Fusion Devices, Jun 2022, E-conference, South Korea. 2022, Nuclear Materials and Energy. cea-03785360

HAL Id: cea-03785360

<https://cea.hal.science/cea-03785360>

Submitted on 23 Sep 2022

HAL is a multi-disciplinary open access archive for the deposit and dissemination of scientific research documents, whether they are published or not. The documents may come from teaching and research institutions in France or abroad, or from public or private research centers.

L'archive ouverte pluridisciplinaire **HAL**, est destinée au dépôt et à la diffusion de documents scientifiques de niveau recherche, publiés ou non, émanant des établissements d'enseignement et de recherche français ou étrangers, des laboratoires publics ou privés.

Numerical modeling of the impact of leakage under divertor baffle in WEST

H. Yang¹, G. Ciraolo¹, J. Bucalossi¹, H. Bufferand¹, N. Fedorczak¹, P. Tamain¹, G. Falchetto¹, N. Rivals¹, J.P. Gunn¹, Y. Marandet², B. Pégourié¹, S. Vartanian¹, and the WEST team*

¹ CEA, IRFM, F-13108 Saint Paul-lez-Durance, France

² Aix Marseille University, CNRS, PIIM, Marseille, France

* See <http://west.cea.fr/WESTteam>

Abstract

In WEST experimental campaign C5, the divertor pumping capability has been improved by sealing the space between the divertor outer baffle and the vacuum vessel. It is expected that the degree of baffle leakage influences the transport of neutral particles inside the main chamber, which affects the detachment onset. Knowing the exact impacts of leakage and understanding the physical processes behind it are helpful for the study and control of plasma detachment. We investigate the impact of leakage by performing transport simulations through SOLEDGE-EIRENE code considering several cases with different leakage levels. Starting from the basic simulation case, non-constant radial transport coefficients obtained by the feedback control method are applied to achieve a better match with the experimental one (#54903) in L-mode. Based on the basic case, the evolution of plasma regimes from sheath limited regime to detached one in different wall geometries has been studied by ramping the upstream density. The numerical results show that the cases with closed or reduced leakage under the baffle have better performance in trapping the neutral particles and higher neutral pressure near the baffle. The neutral compression ratio is increased by a factor up to 4, leading to more significant momentum and power dissipation in the divertor, thus lowering the detachment threshold in $n_{e,sep}$ by up to 16%. At the same time, a much higher gas puff rate by a factor up to 22 is needed to maintain an equivalent $n_{e,sep}$ level in the case without or reduced leakage. For all the cases here, there exist characteristic parameters on which the baffle closure has no obvious influence on their value when plasma starts to detach. The evolution of radiator height as a function of target temperature shows no sensitivity to the leakage, which gives some insight into the stable detachment control strategy in the future. Finally, simulation results are compared with available neutral pressure measurements from WEST campaigns to verify the predictions from the simulation.

Keywords: detachment, SOL, divertor, baffle closure, leakage effect, numerical modelling

1. Introduction

In the next generation of magnetized fusion devices (ITER, DEMO), more than 80% of the exhaust power has to be dissipated before impacting the divertor target plates, the final heat flux loaded on the wetted area should maintain the peak value below 10MW/m² [1]. Plasma detachment is one of the explored solutions for spreading power over larger surfaces through radiation and keeping target heat loads at manageable levels [2]. Therefore, it is important to have a better understanding of the properties of the detached regime. Wall geometry and especially baffle configuration can significantly influence detachment properties due to its effect on the plasma-neutrals interactions in the divertor region. Higher neutral pressure can be achieved in baffled divertor because fewer neutral particles can escape from it. The plasma-neutrals interaction increases with higher neutral pressure, leading to more momentum and power loss for the plasma in the baffled divertor [3]. Recent numerical and experimental studies, in particular on TCV, show that both inner and outer baffles have local effects of trapping the neutral particles, but the global effect of the outer baffle is quantitatively stronger than the one of the inner baffle [4]. However, it

is extremely difficult to generalise these results obtained on a specific device, as the wall and magnetic geometry are strongly varying from one device to another. In this respect, additional results from other devices are very helpful to progress toward a deeper comprehension of the impact of such geometries on plasma-neutrals interaction and consequently on plasma behaviour.

The WEST (W-tungsten Environment in Steady-state Tokamak) is the transformation of the Tore Supra tokamak from a carbon limiter to a tungsten divertor configuration [5]. In recent experiment campaign C5, the space between the divertor baffle and the vacuum vessel has been sealed. It is expected that this modification in baffle configuration improves the divertor pumping capability because of higher neutral pressure in the region under the baffle and close to the pump, allowing for better control of the detached plasma regime. The sealed leak under the baffle can influence the divertor closure which refers to the degree of neutral particles escaping from the divertor [6]. For studying the impact of the wall geometries on divertor behaviour, several studies have already been performed in other tokamak devices, for example, DIII-D [7–12], TCV [4, 13, 14], ASDEX-Upgrade [15], JET [16–18], EAST [19, 20], and

JT-60U [21]. One common observation is that a better divertor closure results in a decrease of separatrix density required for detachment.

In the present article, we discuss the impact of leakage based on considering several sizes of the leakage in the numerical investigation and then comparing with few available experimental data to get more insight into the particle recirculation inside WEST. This article is organised as follows. In Section 2, we present the simulation setups, the wall and magnetic geometries we have considered. In Section 3, we analyse the simulation results, focusing on the detachment threshold, transport of neutrals, and evolution of radiation front until detachment. In Section 4, we discuss about the parameter sensitivity under the impact of leakage. In Section 5, the simulation results will be compared with experimental results to get further insight into the neutral circulation in WEST. We conclude in Section 6.

2. Modeling of background plasma in a WEST discharge

The WEST shot #54903 in L-mode of the C4 campaign is selected as a reference case for the numerical modeling work. We focus on the time when the plasma is relatively stable at $t_{\text{flattop}} = 8\text{s}$ (time since the start of the pulse). The operational parameters are shown in Table 1. The magnetic configuration and wall geometry are shown in Figure 1a with the gas puff position set inside the PFR (private flux region), and the pump position set under the baffle. As this experimental shot case is performed with low heating power and inside a W-covered chamber, the influence of impurities can be very small.

Major radius R_0 (m)	2.5
Minor radius a (m)	0.4
Plasma current I_p (MA)	0.5
Toroidal field B_t (T) @ R_0	3.6
Ohmic heating power $P_{\text{in,Ohmic}}$ (MW)	0.52
ICRH heating power $P_{\text{in,ICRH}}$ (MW)	0.24
Core radiated power $P_{\text{rad}}^{\text{core}}$ (MW)	0.22
Upstream separatrix density $n_{e,\text{sep}}$ (10^{19}m^{-3})	1.64
Gas puff rate ($\text{Pa m}^3 \text{s}^{-1}$)	0.719

Table 1: The operational parameters of WEST shot case #54903 at $t_{\text{flattop}} = 8\text{s}$ in C4 campaign.

The simulation work in this paper was done through SOLEDGE-EIRENE transport code based on merging the transport code SOLEDGE2D [22] and turbulence code TOKAM3X [23]. It inherits the specificity of SOLEDGE2D, using the immersed boundary condition technique called ‘penalization’, in order to recover the Bohm boundary conditions under flexible wall geometry, enabling simulations of the plasma up to the wall [24]. Here, toroidally symmetric 2D simulations

without turbulence were performed to simplify the calculation and facilitate the analysis of the results.

We try to reproduce an L-mode plasma background and make it match with the experimental case. For the simulation setups of the basic case, we apply the baffle closed wall geometry and LSN magnetic configuration as shown in Figure 1a. Deuterium gas fuelling is the only external source of particles. We consider only pure deuterium plasma and no drift effects. In this way, we can analyse the impact of leakage from the aspect of neutrals’ transport with other effects isolated. The influence of drift and impurities will be investigated in the near future. Typical values $\alpha_e = 0.2$ and $\alpha_i = 2$ are applied in the flux limiter [25]. Other detailed setups are shown in Table 2. Here $P_{\text{in,total}}$ is the total input power, $P_{\text{rad}}^{\text{core}}$ is the core radiated power inside the core-edge-interface (CEI). The $P_{\text{in,domain}}$ is calculated by subtracting the $P_{\text{rad}}^{\text{core}}$ (about 0.22 MW, evaluated by bolometer method [26]) from the $P_{\text{in,total}}$ ($P_{\text{in,Ohmic}} + P_{\text{in,ICRH}} \approx 0.76\text{MW}$, in Table 1), as we have no impurity in the simulations here, the radiated power in computational domain is expected to be lower compared to reality, so the final input power of calculation domain is set as 0.5MW. The input power is equally shared between electrons and ions from the core boundary. $R_{\text{wall}} = 1$ is the recycling coefficient of the main chamber wall, $R_{\text{pump}} = 0.95$ is the recycling coefficient of the pump. D_{\perp} is the cross-field mass diffusivity perpendicular to the flux surface, ν_{\perp} is the radial momentum diffusivity, $\chi_{\perp,e}$ and $\chi_{\perp,i}$ are the radial heat flux diffusivity for electrons and ions, respectively.

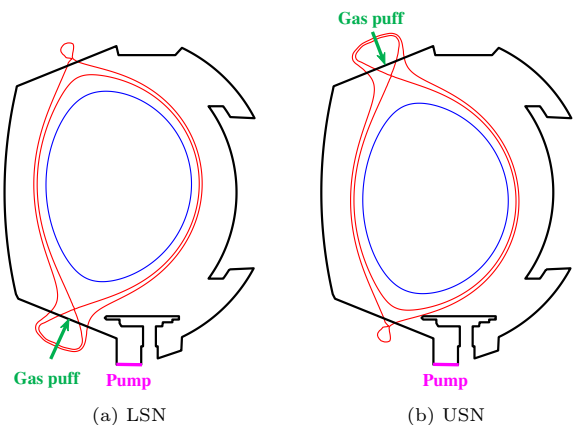


Figure 1: (a) WEST LSN magnetic configuration comes from the experiment shot #54903 at $t_{\text{flattop}} = 8\text{s}$, with wall geometry in the poloidal cross-section. (b) WEST USN magnetic configuration which is symmetrical with LSN magnetic configuration along the mid-plane, with the same wall geometry in the poloidal cross-section. In both sub-figures, the black solid curve represents the chamber wall, the red solid curves represent the separatrix, the blue solid curve represents the core boundary, the green arrow represents the gas puff position, the magenta line represents the pump position.

The feedback control of the anomalous transport coefficients in the radial direction and gas fuelling located in the PFR is activated simultaneously to obtain close upstream profiles compared with the experiment. In shot #54903, we have an upstream electron density profile on the Outer Mid-Plane (OMP) from reflectometry diagnostic, but the temperature profile is unavailable. For this reason, we only control D_{\perp} in this simulation,

Plasma composition	Pure deuterium
Upstream separatrix electron density $n_{e,sep}$ (10^{19}m^{-3})	1.64
Input power of calculation domain (MW)	$P_{in, domain} = P_{in, total} - P_{rad}^{core} \approx 0.5$
Recycling coefficients	$R_{wall} = 1, R_{pump} = 0.95$
Transport coefficients (m^2s^{-1})	(D_{\perp} in Figure 2, $\nu_{\perp} = 0.3, \chi_{\perp, e} = \chi_{\perp, i} = D_{\perp}/0.3$)
Number of particles in EIRENE	200000

Table 2: The setup parameters for the simulation of basic case in SOLEDGE-EIRENE.

and suppose $\chi_{\perp, e} = \chi_{\perp, i} = D_{\perp}/0.3$, to maintain proportional relationship with the WEST classic L-mode setups $D_{\perp} = 0.3, \chi_{\perp, e} = \chi_{\perp, i} = 1$. The radial momentum diffusivity is constant as $\nu_{\perp} = 0.3$. The final converged D_{\perp} profile at the OMP is shown in Figure 2. In the calculation domain, the transport coefficients are poloidally constant, except for the location inside the PFR, transport coefficients are the same as the value at the separatrix.

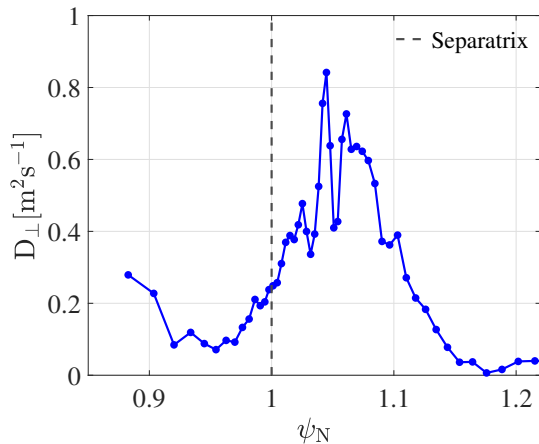


Figure 2: The evolution of D_{\perp} as a function of ψ_N at the OMP, controlled by the feedback function to match with the experimental density profile.

After the simulation is converged, the 2D plots of electron density and temperature in the calculation domain of the basic case are shown in Figure 3. Its upstream and target profiles are compared with the experimental results as shown in Figure 4 and 5. We can see a good match between the experiment and simulation for both upstream and downstream profiles. In the shot #54903 during the time from 7s to 9s, the upstream $n_{e,sep}$ is relatively stable while the gas puff rate keeps decreasing linearly indicating a gradually saturated wall. The gas puff rate at $t_{flattop} = 8\text{s}$ is around $0.719\text{Pa}\cdot\text{m}^3\text{s}^{-1} \approx 3.47 \times 10^{20}\text{D atoms s}^{-1}$ which can represent the averaged value that maintain the stable state. In the simulation, we need to maintain upstream separatrix electron density $n_{e,sep} = 1.64 \times 10^{19}\text{m}^{-3}$ through gas puff feedback, and the averaged gas puff rate is $3.10 \times 10^{20}\text{D atoms s}^{-1}$. So the simulation case has a deuterium gas puff rate close to the experimental one.

One needs to notice that, the simulation of the basic case is performed with closed baffle which is not fully consistent with the situation of the experimental one as

the shot case#54903 in C4 campaign also had leakage problem. Later analysis in Section 3 shows that the simulation supposes to have a higher target temperature and parallel heat flux when leakage is introduced (due to less momentum and power dissipation). If we consider this aspect into account, the simulation of the basic case with closed baffle has the potential to achieve an even better match with the experimental one for the target profiles.

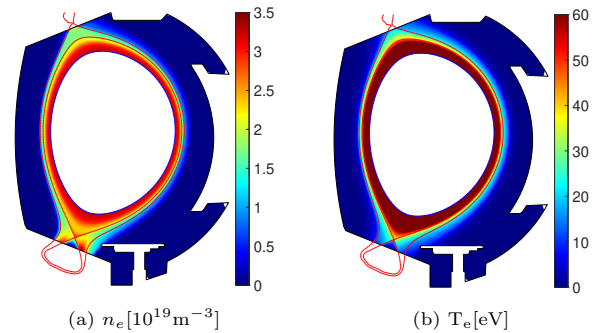


Figure 3: 2D plots of WEST basic simulation case (matched with experiment) for electron density, electron temperature.

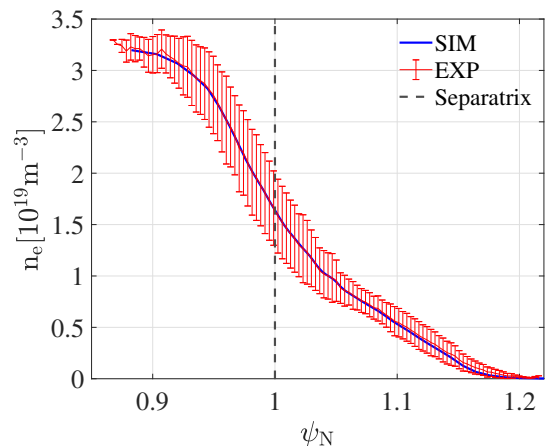


Figure 4: Radial profile of electron density at the OMP, comparing between the experimental measurements (reflectometry method, red curve with error bars) and the SOLEDGE-EIRENE simulation (blue curve). The dashed line represents the position of separatrix. ψ_N is the normalised poloidal magnetic flux.

Starting from the basic case, different baffle configurations from closed to open (baffle removed) are applied to make the simulation to evaluate the effects of baffle leakage, as shown in Figure 6. The leakage problem in WEST was due to the toroidal discontinuity of divertor baffle. Here, we put the leakage position at the

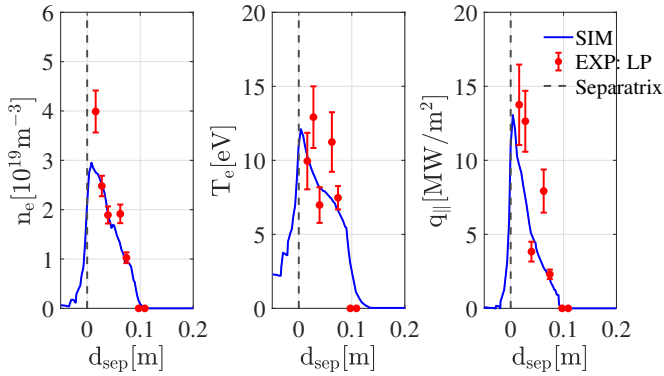


Figure 5: The profiles of electron density, electron temperature, parallel heat flux on the outer target, comparing between the experimental measurements (Langmuir Probes (LP), red dot with error bar) and the SOLEDGE-EIRENE simulation (blue curve). The dashed line represents the position of separatrix. d_{sep} is the radial distance from the outer strike point, negative values are in the PFR, positive values are in the SOL.

bottom of the baffle to facilitate the 2D simulation, the leakage level before the WEST experimental campaign C5 is supposed to be close to or smaller than that of the baffle with small leakage, Figure 6b. Among the five baffle configurations, four of them are just different at the bottom part of the baffle but have the same top part in order to exclude the possible influence of recycling on the baffle [13], the remaining one removed the baffle completely. In addition, the USN case with the magnetic configuration symmetrical to the LSN one along the mid-plane shown in Figure 1b has been considered because it is easier to investigate the effects of open and closed baffle through the comparison between LSN closed baffle discharge and USN no baffle discharge when carrying out the experiments. For this purpose, the USN case has the same wall geometry as LSN closed baffle case, with the gas puff position inside the PFR, but the pump remained at the bottom part as it can not be changed in WEST.

The meshes built based on different configurations (different baffle configurations, LSN and USN magnetic configurations) are not exactly the same and may have a slight difference in partial cell size. Thus, the one-dimensional interpolation method needs to be used if we want to apply the non-constant radial transport coefficient (Figure 2) in each configuration. However, the interpolation procedure can introduce small difference between the radial transport coefficient profiles that are finally applied in each case. To make a fair comparison between all the cases, we apply the WEST classic L-mode transport coefficient setups $D_{\perp} = 0.3$, $\chi_{\perp,e} = \chi_{\perp,i} = 1$ for the later simulations, as the mean value of non-constant radial transport coefficient D_{\perp} is around 0.3, the classic value can be thought as a good choice. In this situation, we also change the input power to 0.45MW, to keep the target profile of the baffle closed case has a good match with the experimental one (not shown here). These procedures can at least keep the main conclusion for the impact of leakage consistent with the ideal situation. From the comparison of the simulation results in Section 3, we understand that the influence of different pump positions relative to

the outer strike point is small, and the USN no baffle case shows characteristics consistent with LSN no baffle case. So it's acceptable to compare LSN closed baffle discharge and USN no baffle discharge directly, and provides support for the subsequent experimental verification in Section 5. The influence of pump position in LSN and USN will be investigated in the future.

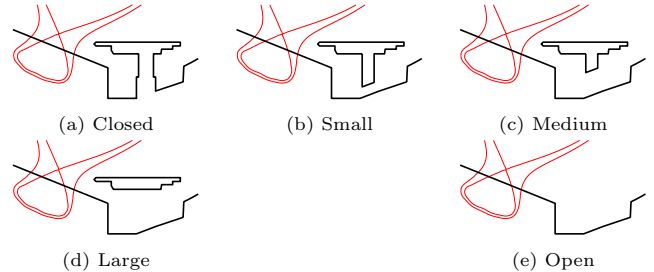


Figure 6: Baffle configurations considered in the SOLEDGE-EIRENE simulations: (a) the case with closed baffle, (b) the case with small leak under the baffle, (c) the case with medium leak, (d) the case with big leak and (e) the case with the baffle removed, in other words, open baffle.

In order to make the simulation results cover different plasma states, from the sheath limited regime to the detached regime, the density scan is applied for a low input power case going from $n_{e,\text{sep}} = 1.0 \times 10^{19} \text{ m}^{-3}$ to $3.0 \times 10^{19} \text{ m}^{-3}$. As shown in Figure 7, the sensitivity of gas puff rate in each case can be obviously influenced by different sizes of leakage, leading to a specific range of operational gas puff rate in each case. However, the range of operational upstream $n_{e,\text{sep}}$ is overall limited below $3.0 \times 10^{19} \text{ m}^{-3}$, without degrading the core plasma or inducing a radiative collapse. All the cases share the same setups besides the differences in wall geometry and in operational gas puff rate during the upstream $n_{e,\text{sep}}$ scan.

3. Assessment of leakage effects

In this section, we investigate the impact of the level of baffle leakage on plasma behaviour and transport of neutrals. We start with the analysis of the detachment threshold.

3.1. Detachment threshold

The simulation result is always time-dependent in SOLEDGE-EIRENE. Here, we analyse only the final steady-state result. To reduce the effects of the oscillation from Monte Carlo simulation on the final results, we increase the number of particles used in EIRENE to 2×10^5 . After the simulation is converged, the data set used for analysis is obtained by sampling 20 data every 1×10^4 iterations (time step $dt \approx 2 \times 10^{-8} \text{ s}$) in SOLEDGE. The results with error bars in some figures show average value and the standard deviation of its data set.

In Figure 7, we can observe that the range of operational gas puffing rate is the broadest in the case with closed baffle. The more leakage under the baffle, the narrower the range of operational gas puffing rate. In addition, the upstream $n_{e,\text{sep}}$ ramped up with increasing gas puff rate in the simulations of each case.

In the two-point model's prediction [2], the parallel electron flux on the target $\Gamma_{e,t}$ increases proportionally to $n_{e,sep}^2$ in high-recycling regime. After reaching a threshold value of $n_{e,sep}$, $\Gamma_{e,t}$ rolls over and the plasma steps into the detached regime. The threshold value of $n_{e,sep}$ corresponding to the rollover of $\Gamma_{e,t}$ is called the detachment threshold in upstream $n_{e,sep}$. The detachment threshold can also be expressed with respect to gas puff rate. The profiles of peak $\Gamma_{e,t}$ on the outer target as a function of gas puff rate and as a function of upstream $n_{e,sep}$ are shown in Figure 8 and Figure 9 respectively. It can be observed that the smaller degree of the leakage, the higher is the detachment threshold in gas puff rate, but the lower detachment threshold in upstream $n_{e,sep}$. The relative decrease in upstream separatrix density threshold is much smaller than the relative increase in gas puff rate threshold with reducing leakage under the baffle.

Also, the USN open case has a very close detachment threshold compared to the LSN open one, and their peak $\Gamma_{e,t}$ profiles are matched in low upstream $n_{e,sep}$ until the detachment happens. After the rollover of peak $\Gamma_{e,t}$, the USN open case has a higher $\Gamma_{e,t}$ value on the outer target than that of the LSN open case under the same upstream $n_{e,sep}$. The USN open case shows some consistent characteristics with the LSN open case, but the USN one seems to be more open than LSN one after surpassing the detachment threshold.

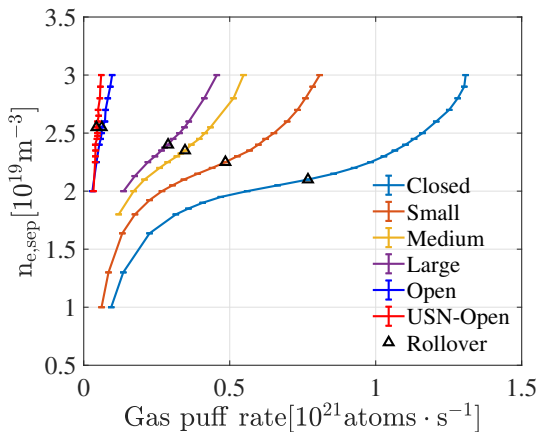


Figure 7: The evolution of the upstream separatrix electron density $n_{e,sep}$ as a function of the gas puff rate for the six cases (five LSN cases with baffle from closed to open and one USN case with no baffle in the upper divertor) under consideration. The black triangle on each curve marks point when the rollover of $\Gamma_{e,t}$ happens as shown in Figure 8.

3.2. Impact of leakage level on transport of neutrals

For the cases with leakage under the baffle, some neutrals can escape to the low field side of the main chamber through the leak position under the outer baffle since they are not magnetized. To study more details about the transport of neutrals, we made a 2D plot comparison between two LSN cases, one with closed baffle and another with small leak under the baffle, as shown in Figure 10. Two cases have the same gas puff rate = 2.25×10^{20} D atoms s^{-1} . The result shows that in the presence of the leakage, the neutral density in the low field side increases by a factor from 2.5

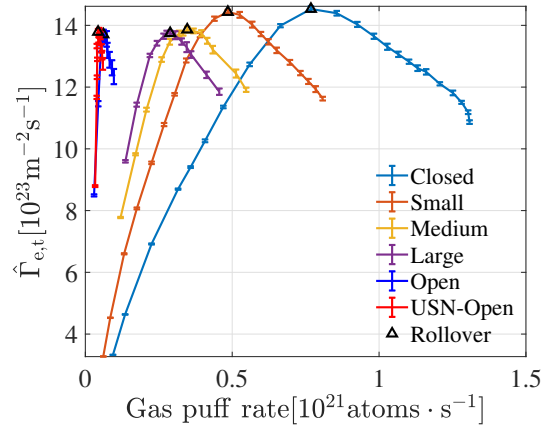


Figure 8: The evolution of peak electron particle flux $\Gamma_{e,t}$ on the outer target as a function of gas puff rate for the six cases under consideration, the values corresponding to the rollover have been marked by black triangles.

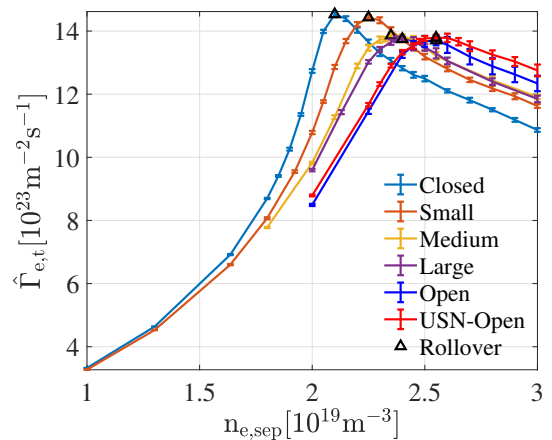


Figure 9: The evolution of peak $\Gamma_{e,t}$ on the outer target as a function of upstream $n_{e,sep}$ for the six cases under consideration, the rollover positions have been marked by black triangles.

to 6. When there are more neutral ionization sources nearby the separatrix, the upstream $n_{e,sep}$ will increase accordingly. That's why the case with leak has higher upstream $n_{e,sep}$ compared with the closed case under the same gas puff rate. Vice-versa, the case with closed baffle needs to increase the gas puff rate to maintain the same upstream $n_{e,sep}$ as the case with small leak. This is consistent with what we observed in Figure 7. In addition, for the case with leakage, overall less neutral penetration in the confined region can be observed (light blue region in Figure 10c), but when checking the neutral density profile at the OMP, the neutral density is slightly higher from CEI to the separatrix. Further investigations are necessary for understanding the neutral penetration under the impact of leakage.

The neutral compression ratio is used to analyse the impact of leakage quantitatively, it can be defined as the ratio between the neutral pressure on the outer divertor target and that at the near wall outer mid-plane (the point at the OMP and close to the antenna). Here the neutral pressure on the outer divertor target comes from the neutral pressure averaged over the outer target region. A higher neutral compression ratio can be observed in the case with a lower leakage level under the same upstream $n_{e,sep}$, corresponding to a better per-

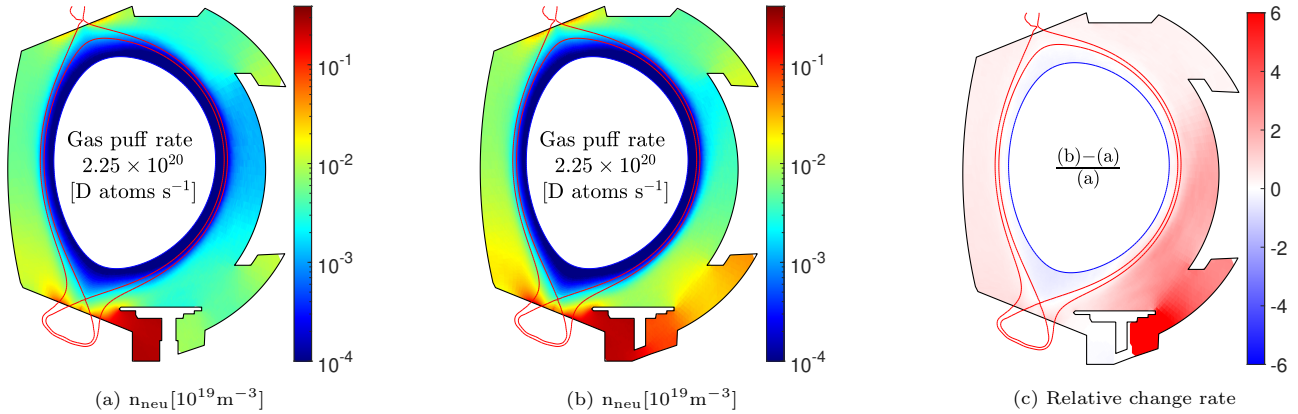


Figure 10: (a) The neutral density n_{neu} distribution in the case with closed baffle. (b) The neutral density n_{neu} distribution in the case with small leak. Both (a) and (b) have the same setup parameters include the same gas puff rate = $2.25 \times 10^{20} \text{ atoms} \cdot \text{s}^{-1}$. (c) The contour of relative change rate in neutral density n_{neu} shows that the leakage under baffle results in the increase of neutral density by a factor of 2.5 - 6 in low field side and of 1.5 in the high field side of the main chamber.

formance of the divertor region in trapping the neutral particles as shown in Figure 11. For two cases with no baffle (LSN open case and USN open case), the compression ratio changes slightly and is around 50 in the upstream $n_{e,\text{sep}}$ range that is covered by the simulation. So we can consider that the compression ratio is not sensitive to the variation of upstream $n_{e,\text{sep}}$ in the two cases. However, in the case with closed baffle, the ratio is increased by a factor up to 4 and changes between 50 and 200, and the compression ratio improved significantly with increasing upstream $n_{e,\text{sep}}$ before the rollover of $\Gamma_{e,t}$. After the rollover, the compression ratio changes slightly, in the end, tend to decrease when the upstream $n_{e,\text{sep}}$ becomes very high. The different behaviours of the compression ratio before and after detachment can be explained as being affected by the different heights of the ionisation front. When the plasma is attached, more and more neutrals are trapped in the divertor region with increasing upstream plasma density $n_{e,\text{sep}}$, and the compression ratio is increased simultaneously. However, when the plasma is detached, the ionisation front moves up off toward the X-point. So, in this situation, it's easier for neutral particles to escape the divertor region, and the restricting effect of the baffle is weakened. Also, the recycling on the baffle tip becomes more important in high upstream $n_{e,\text{sep}}$. Both aspects can explain the decrease of the compression ratio under very high upstream $n_{e,\text{sep}}$.

3.3. Evolution of radiation front

With high $n_{e,\text{sep}}$, a significant increase in radiation level near the divertor is predicted by the SOLEDGE-EIRENE simulation, as shown in Figure 12. It's also observed that the radiation increases very fast: initially, it is mainly distributed near the strike points region on the divertor, then increasing plasma density by ramping the gas puff rate to a higher value, the maximum radiation region moves up off the divertor target, and two radiation centers on the inner and outer leg merged together near X-point in the detached regime. During this process, the fronts of the radiation region close to the target can be defined as detachment fronts, where a steep temperature gradient exists because of volumetric radiation and charge exchange. Several definitions

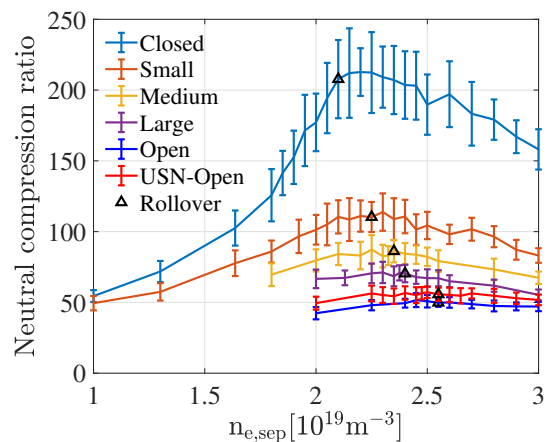


Figure 11: The profiles of the neutral compression ratio (ratio between the average neutral pressure on the outer target and the near wall outer mid-plane position). The black triangle on each curve marks the point when the rollover of $\Gamma_{e,t}$ happens.

of detachment front can be found in the literature. In this paper, we define the front of radiation which encloses an area that has less than 30% reduced radiation compared to the maximum radiation.

The average electron temperature inside the radiation front is evaluated, as shown in Figure 13, together with the peak electron temperature on the outer target. We can observe that the average temperature inside the radiation front is around 4.2 eV and the peak electron temperature on the outer target is around 2.2 eV when $\Gamma_{e,t}$ rollover happens in each case. The average electron temperature inside the radiation front doesn't change much after the radiation front detaches from the target. It means that the region inside the radiation front can maintain a relatively stable temperature of around 4.2 eV after the detachment happens, and the radiation is much more active at this characteristic temperature. In a deep detached case with $n_{e,\text{sep}} = 3 \times 10^{19} \text{ m}^{-3}$, the radiation in the entire calculation domain is mainly from the atom excitation (about 90%) and the volume recombination (about 10%). If we focus on the radiation from the region inside the radiation front, the contribution from the volume recombination will increase to about 24%. The volume recombina-

tion radiation mainly happens in the region near the X-point.

We also evaluated the evolution of the vertical distance between the position of the radiator (radiation peak) and the target, as shown in Figure 14. The distance equals 0 in the attached regime, and then it ramps up with raised upstream $n_{e,sep}$, and can even be higher than the vertical distance between X-point and target in the end. One interesting thing observed is that the radiator height corresponding to the rollover of $\Gamma_{e,t}$ is always around 1.4 cm.

Simulation results above show that there exist rollover characteristic parameters: the peak electron temperature on the outer target about 2.2 eV, the average electron temperature inside the radiation front around 4.2 eV, the vertical distance between the position of the radiator and target about 1.4 cm, on which the baffle closure has no obvious influence. This peak target temperature result is close to what has been observed in the DIII-D experiment, T_e drops to 2 eV when the rollover in peak J_{sat} happened [27]. This phenomenon is probably due to the factors: The ion-neutral interaction happens at T_e from 2 to 5 eV, and plasma recombination happens at T_e below 1 eV [28].

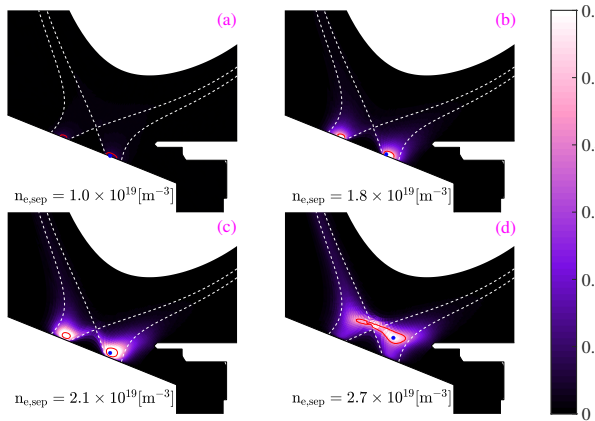


Figure 12: Radiation power [MW/m^3] in the case with closed baffle. With increasing upstream $n_{e,sep}$, the main radiation regions surrounded by the radiation fronts (composed of the points where have 70% of maximum radiation in the calculation domain, marked by red curve) move up off the divertor target, and two radiation centers on the inner and outer leg merged together near the X-point in the deeply detached regime. Four figures [a-d] correspond to four upstream $n_{e,sep}$ marked in Figure 14. The blue dot represents the position where it has the maximum radiation. The white dashed curves represent the separatrix.

4. Parameter sensitivity influenced by the leakage

As we discussed in Section 3.2, the relationship between $n_{e,sep}$ and gas puff rate is indirectly influenced by the baffle configuration, which can have effects on the neutral transport. Thus we can observe a significant difference among the profiles of six cases with different levels of leakage, shown in Figure 7. Another obvious difference exists among the profiles of peak electron temperature on the outer target as a function of $n_{e,sep}$ shown in Figure 13. The target electron temperature as a downstream parameter is influenced by the upstream

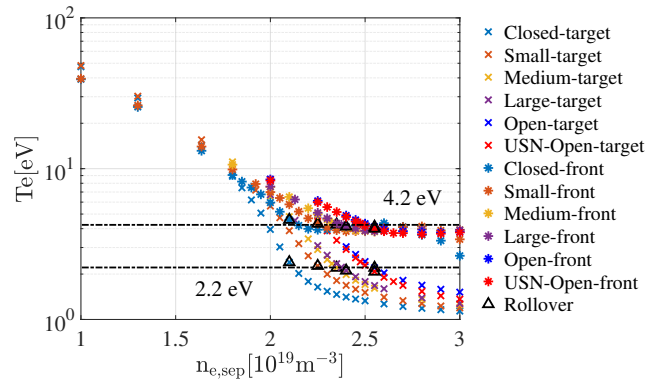


Figure 13: The scatter points of the peak electron temperature on the outer target (marked by crosses) and the average electron temperature inside the radiation front (marked by asterisks). The black triangle on each curve marks the point when the rollover of $\Gamma_{e,t}$ happens.

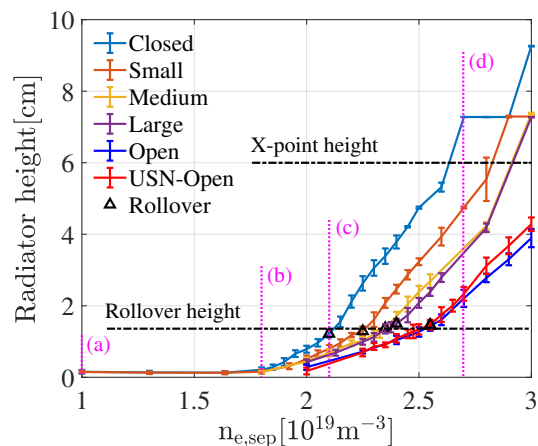


Figure 14: The profiles of the vertical distance between the position of radiator (radiation peak) and target. When $\Gamma_{e,t}$ rollover happens in each case (marked by black triangle), the radiator height is always around 1.4 cm. The X-point height is about 6 cm. The four LSN baffle closed cases marked by magenta columns [a-d] correspond to radiation plots [a-d] in Figure 12.

parameter $n_{e,sep}$ in SOL. In the process from upstream to target, for the cases with reduced leakage, the momentum and power dissipation of plasma increase due to overall higher neutral pressure near the divertor.

However, the relationship between the radiator height and the target electron temperature seems not significantly influenced by the baffle configurations with different leakage levels, as shown in Figure 15, those scatter points are almost distributed around the same curve. This can be explained as the temperature on the target plays a key role in setting the power and momentum dissipation factor due to these processes mainly happen in the region near divertor target. For this reason, the plasma regime is directly related to the target temperature. The levels of leakage, however, play a role in affecting the relationships between the gas fuelling, upstream and target parameters. The insensitivity of radiator height to the leakage when it's as a function of local target temperature can be useful in detachment control. During the real experimental shot, the slight change of distance between the separatrix and the baffle tip (due to instability issues) can also lead to an obvi-

ous change in baffle closure and presents similar effects like the baffle leakage as we discussed in this paper; the transport process between upstream and downstream can be influenced by the leakage. So in the ideal situation, it is preferred to take the parameters near the target (e.g. target temperature) as the input signals when designing the feedback control system which aims to achieve stable detachment.

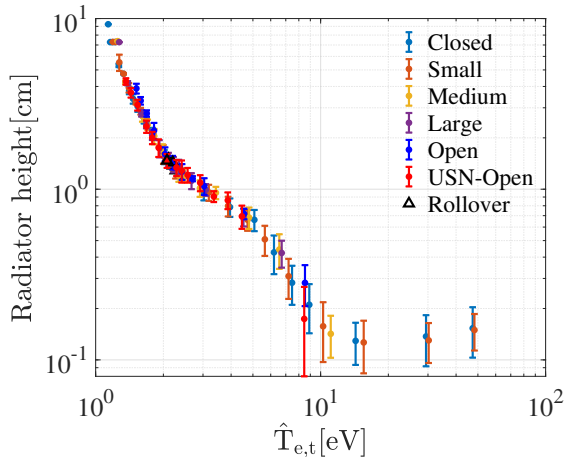


Figure 15: The scatter points of the radiator height as a function of peak $T_{e,t}$ on the outer target.

5. Comparing with experiment

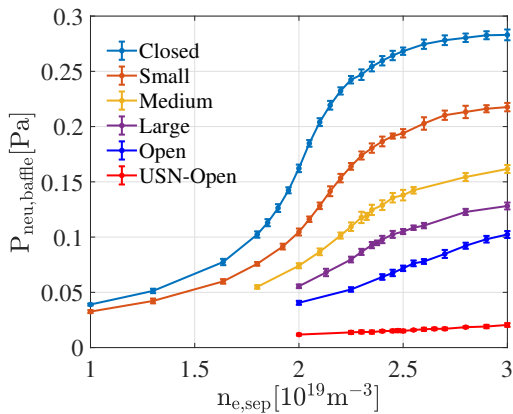


Figure 16: The evolution of neutral pressure under baffle as a function of upstream $n_{e,sep}$.

Results from the SOLEDGE-EIRENE simulation are confronted with four WEST discharges, as shown in Table 3. In WEST experimental campaign C5, the space between the divertor outer baffle and the vacuum vessel was sealed. The experimental data from the LSN shot case in C5 can be considered as baffle closed case when compared with the simulation, the one in C4 can be considered as the case with small leakage. For the case #56923 in C5, we can observe about 50% higher neutral pressure under baffle $P_{neu,baffle}$, 17% higher upstream $n_{e,sep}$ and 13% higher central line integrated density comparing with the case #55077 in C4. Both cases have very close operational parameters. In the prediction of simulation for the neutral pressure under the baffle as shown in Figure 16, the LSN baffle closed

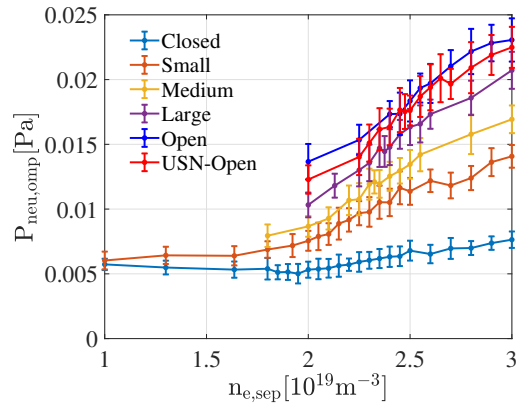


Figure 17: The evolution of neutral pressure at the near wall outer mid-plane position as a function of upstream $n_{e,sep}$.

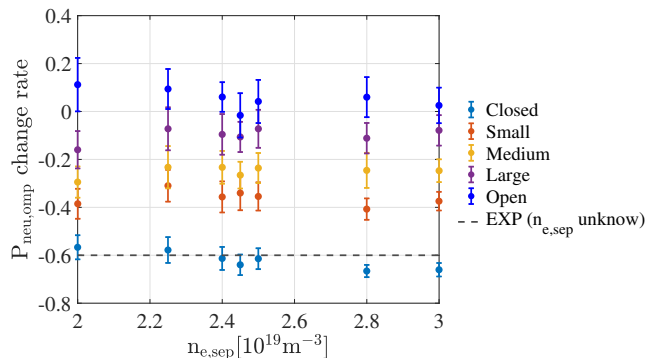


Figure 18: The change rate of the neutral pressure at the near wall outer mid-plane ($(P_{neu,omp}^{LSN} - P_{neu,omp}^{USN})/P_{neu,omp}^{USN}$) as a function of upstream $n_{e,sep}$. The dashed line represent the $P_{neu,omp}$ change rate = -0.6, comparing between #56726 and #56769.

case indeed has higher neutral pressure than the other LSN cases with leakage under the same upstream $n_{e,sep}$ which is consistent with the result given by experiment. However, the neutral pressure under the baffle evolves as a function of $n_{e,sep}$. For this reason, the increase of about 17% in the upstream density can also impact the neutral pressure under the baffle, making it difficult to conclude that the 50% higher neutral pressure under baffle is due to the effect of leakage sealed in the campaign C5. Moreover, other modifications implemented in WEST vacuum vessel between C4 and C5, like the change in the material of limiter bumpers, could impact the neutral density and pressure. For this reason, it is very challenging to estimate the impact of the leakage by comparing C4 and C5 discharges.

We also need to notice that the absolute values of neutral pressure under the baffle and the one at the near wall outer mid-plane are much higher in the simulations (Figure 16 and 17) than in the experiment (Table 3) by a factor up to 25. The neutral pressure difference between simulation and experiment is possibly due to two factors: First, different measure positions. In experiment, the neutral pressure is measured after the pipe conduction, but in simulation, the P_{neu} is obtained directly from the locations (the region near the wall at the OMP and the region not far below the baffle). This factor can cause the underestimate of neutral pressure in experiment; Second, the pure D simulation case also shows a higher P_{neu} compared to the simulation case

Shot case	55077	56923	56726	56769
Campaign	C4	C5	C5	C5
Configuration	LSN	LSN	LSN	USN
Plasma current I_p (MA)	0.5	0.5	0.4	0.4
Toroidal field B_t (T)	3.6	3.7	3.2	3
Heating power $P_{in,total}$ (kW)	150	140	365	375
Central line integrated density ($1e19/m^2$)	4	4.5	3	3
Upstream separatrix density $n_{e,sep}$ ($1e19/m^3$)	1.8 ± 0.25	2.1 ± 0.25	-	-
$P_{neu,omp}$ (mPa)	0.2	0.2	0.2	0.5
$P_{neu,baffle}$ (mPa)	10	15	6	-
$t_{flattop}$ (s)	15	15	6	6

Table 3: The data of experiment cases, $P_{neu,omp}$ represent the average neutral pressure at the near wall outer mid-plane position, $P_{neu,baffle}$ represent the average neutral pressure under baffle.

with impurities(C or N). In pure D simulation, the neutral particles play an important role in the momentum and power dissipation of plasma. When the impurities particles are introduced into the plasma, they are much more effective in dissipating the power than the D atoms. In the case of the same energy dissipation, the pressure of D atoms and the total pressure of neutral particles required is greatly reduced under the effects of impurity. These aspects will be investigated further in future studies. So the $P_{neu,omp}$ measured in the experiment can not compare directly with the data from simulation as they are not in the same order of magnitude.

To make a fair comparison, we choose two cases in the same campaign C5, one is LSN case #56726, and another one is USN case #56769. Both are pure Ohmic heating cases, with very close central line integrated density and operational parameters. However, there was no diagnostic available to evaluate the neutral pressure in the upper divertor, and the reflectometry density measurement (used to evaluate the $n_{e,sep}$) on the outer mid-plane was not performed in the two cases. A workaround is to compute the change rate of the neutral pressure at the near wall outer mid-plane $P_{neu,omp}$ for each LSN case, the change rate is defined as $(P_{neu,omp}^{LSN} - P_{neu,omp}^{USN})/P_{neu,omp}^{USN}$. For the cases with baffle, the change rate is normally negative. It represents the decrease of neutral pressure in the far SOL when the baffle is introduced as the baffle can limit the leakage of neutral particles from the divertor, thus lowering the neutral pressure in the far SOL as discussed in Section 3.2. The baffle with less leakage can have a better effect in limiting the neutral particles, leading to lower $P_{neu,omp}$. For this reason, we can see the baffle closed case has the lowest neutral pressure at the near wall outer mid-plane compared with other cases, as shown in Figure 17. Here we compare the LSN baffled closed case and USN case directly because the USN case can be considered as LSN no baffle case, and they have consistent characteristics as discussed in Section 2.

The reasons for using the $P_{neu,omp}$ change rate to analyse the impact of leakage in the experiment are: First, this parameter shows insensitivity to the changes of upstream $n_{e,sep}$ as shown in Figure 18. This is important because measurements of upstream conditions are not always available in the experimental discharges;

Second, it's hard to reproduce the plasma in the simulation that has the same order of magnitude of P_{neu} as in the experiment, this part has been discussed before. The $P_{neu,omp}$ change rate can be an ideal parameter to evaluate the tendency that happened in the simulation and experiment under the effects of leakage.

Figure 18 shows the $P_{neu,omp}$ change rate calculated by simulation cases and the value from selected experimental cases as a reference. It can be observed that the reference value given by the experiment matches with the prediction of SOLEDGE-EIRENE when the $P_{neu,omp}$ change rate is calculated between the baffle closed cases and the USN case. This is consistent with the fact that we have a baffle closed divertor in campaign C5 of WEST.

The diagnostics for neutral pressure measurements have been improved since the C5 campaign, with better measurement accuracy and more measurement positions (the upper divertor is included). A more detailed comparison with simulation results will be possible for future experiments, and this aspect will be investigated further.

6. Conclusion

The impact of wall geometry (characterized by different levels of leakage under the divertor baffle) on detachment properties in WEST is investigated using the SOLEDGE-EIRENE transport code. We start by reproducing an L-mode plasma background and making it match the reference one from the experiment by specifying the boundary conditions and applying radial varying transport coefficients obtained by the feedback control method. Based on the basic case, the evolution of plasma regimes from sheath limited regime to detached one in different wall geometries has been studied by ramping the upstream density.

Simulation results show that the case with less leakage has better performance in trapping the neutral particles and has higher neutral pressure near the target, leading to greater power dissipation in the divertor, thus decreasing the detachment threshold in upstream separatrix density. However, to obtain the same upstream separatrix density in the case with less leakage, one needs to ramp the gas puff rate to a higher value due to fewer ionization sources nearby the separatrix. Concerning the threshold refers to the rollover of peak

electron particle flux $\Gamma_{e,t}$, we can observe that the relative decrease in upstream separatrix density threshold is much smaller than the relative increase in gas puff rate threshold with reducing leakage under the baffle. In addition, the evolution of the radiation front has been investigated: The radiation front moves up off the divertor target with high enough upstream $n_{e,sep}$ and two radiation centers on the inner and outer leg merged together near X-point in the deeply detached regime. There exist rollover characteristic parameters: the peak electron temperature on the outer target about 2.2 eV, the average electron temperature inside the radiation front around 4.2 eV, the vertical distance between the position of radiator and target about 1.4 cm, on which the baffle closure has no obvious influence.

The sensitivity of the detachment process to multiple parameters (e.g. upstream density, target plasma temperature) shows a different level of impact from leakage, the impact can be neglected when it's as a function of the target temperature. Controlling a stable detachment through analysing the diagnostic signal of target parameters can be a preferred choice when operating future devices. Finally, simulation results are confronted with experimental data from the configurations USN and LSN. The experimental results show good consistency with the prediction of SOLEDGE-EIRENE code in the aspect of $P_{neu,omp}$ change ratio. There exists a large discrepancy in absolute neutral pressure measurements between experiment and simulation, possibly due to different measurement positions or the influence of impurities. This problem will be investigated in the near future.

Acknowledgements

This work has been carried out within the framework of the EUROfusion Consortium, funded by the European Union via the Euratom Research and Training Programme (Grant Agreement No 101052200 — EUROfusion). Views and opinions expressed are however those of the author(s) only and do not necessarily reflect those of the European Union or the European Commission. Neither the European Union nor the European Commission can be held responsible for them.

References

- [1] R. Pitts, et al., Status and physics basis of the iter divertor, *Physica Scripta* 2009 (2009) 014001.
- [2] P. C. Stangeby, et al., The plasma boundary of magnetic fusion devices, volume 224, Institute of Physics Pub. Philadelphia, Pennsylvania, 2000.
- [3] A. Leonard, Plasma detachment in divertor tokamaks, *Plasma Physics and Controlled Fusion* 60 (2018) 044001.
- [4] D. Galassi, et al., Numerical investigation of optimal divertor gas baffle closure on TCV, *Plasma Physics and Controlled Fusion* 62 (2020) 115009.
- [5] J. Bucalossi, et al., The west project: Testing iter divertor high heat flux component technology in a steady state tokamak environment, *Fusion Engineering and Design* 89 (2014) 907–912.
- [6] A. Loarte, Effects of divertor geometry on tokamak plasmas, *Plasma Physics and Controlled Fusion* 43 (2001) R183–R224.

- [7] L. Casali, et al., Neutral leakage, power dissipation and pedestal fueling in open vs closed divertors, *Nuclear Fusion* 60 (2020) 076011.
- [8] H. Guo, et al., First experimental tests of a new small angle slot divertor on DIII-d, *Nuclear Fusion* 59 (2019) 086054.
- [9] M. Shafer, et al., Dependence of neutral pressure on detachment in the small angle slot divertor at diii-d, *Nuclear Materials and Energy* 19 (2019) 487–492.
- [10] A. L. Moser, et al., The effect of divertor closure on detachment onset in diii-d, *Nuclear Materials and Energy* 19 (2019) 67–71.
- [11] L. Casali, et al., Modelling the effect of divertor closure on detachment onset in diii-d with the solps code, 2018.
- [12] L. Casali, et al., The effect of neutrals in the new sas divertor at diii-d as modelled by solps, *Nuclear Materials and Energy* 19 (2019) 537–543.
- [13] O. Février, et al., Divertor closure effects on the tcv boundary plasma, *Nuclear Materials and Energy* 27 (2021) 100977.
- [14] H. Reimerdes, et al., Initial TCV operation with a baffled divertor, *Nuclear Fusion* 61 (2021) 024002.
- [15] R. Neu, et al., The ASDEX upgrade divertor IIb—a closed divertor for strongly shaped plasmas, *Nuclear Fusion* 43 (2003) 1191–1196.
- [16] A. Loarte, et al., Plasma detachment in JET mark i divertor experiments, *Nuclear Fusion* 38 (1998) 331–371.
- [17] J. T. (prepared by R.D Monk), Recent results from divertor and scrape-off layer studies at JET, *Nuclear Fusion* 39 (1999) 1751–1762.
- [18] L. Horton, et al., Studies in JET divertors of varied geometry. i: Non-seeded plasma operation, *Nuclear Fusion* 39 (1999) 1–17.
- [19] H. Si, et al., Modeling the effect of divertor closure on plasma detachment for new divertor design of EAST by SOLPS, *Plasma Physics and Controlled Fusion* 61 (2019) 095007.
- [20] Y. Q. Tao, et al., Impact of divertor closure on edge plasma behavior in EAST h-mode plasmas, *Plasma Physics and Controlled Fusion* 63 (2021) 065004.
- [21] N. Asakura, et al., Heat and particle transport of SOL and divertor plasmas in the w shaped divertor on JT-60u, *Nuclear Fusion* 39 (1999) 1983–1994.
- [22] H. Bufferand, et al., Numerical modelling for divertor design of the WEST device with a focus on plasma–wall interactions, *Nuclear Fusion* 55 (2015) 053025.
- [23] P. Tamain, et al., The tokam3x code for edge turbulence fluid simulations of tokamak plasmas in versatile magnetic geometries, *Journal of Computational Physics* 321 (2016) 606–623.
- [24] H. Bufferand, et al., Three-dimensional modelling of edge multi-component plasma taking into account realistic wall geometry, *Nuclear Materials and Energy* 18 (2019) 82–86.
- [25] G. Ciraolo, et al., Fluid and kinetic modelling for non-local heat transport in magnetic fusion devices, *Contributions to Plasma Physics* 58 (2018) 457–464.
- [26] G. Ciraolo, et al., First modeling of strongly radiating west plasmas with soledge-eirene, *Nuclear Materials and Energy* 20 (2019) 100685.
- [27] A. Moser, et al., Separating divertor closure effects on divertor detachment and pedestal shape in diii-d, *Physics of Plasmas* 27 (2020) 032506.
- [28] S. Allen, et al., Radiative divertor and scrape-off layer experiments in open and baffled divertors on diii-d, *Nuclear Fusion* 39 (1999) 2015.